Wave packet and statistical quantum calculations for the He + NeH+ → HeH+ + Ne reaction on the ground electronic state

Debasish Koner, Lizandra Barrios, Tomás González-Lezana, and Aditya N. Panda

Citation: The Journal of Chemical Physics **141**, 114302 (2014); doi: 10.1063/1.4895567

View online: http://dx.doi.org/10.1063/1.4895567

View Table of Contents: http://scitation.aip.org/content/aip/journal/jcp/141/11?ver=pdfcov

Published by the AIP Publishing

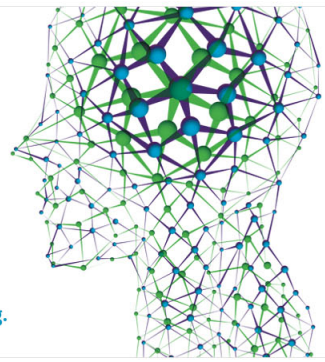

Wave packet and statistical quantum calculations for the He + NeH^+ → HeH^+ + Ne reaction on the ground electronic state

Debasish Koner,[1] Lizandra Barrios,[2] Tomás González-Lezana,[2,a)] and Aditya N. Panda[1,b)]
[1]*Department of Chemistry, Indian Institute of Technology Guwahati, Guwahati 781039, India*
[2]*Instituto de Física Fundamental, C.S.I.C., Serrano 123, Madrid 28006, Spain*

(Received 30 July 2014; accepted 2 September 2014; published online 17 September 2014)

A real wave packet based time-dependent method and a statistical quantum method have been used to study the He + NeH^+ (v, j) reaction with the reactant in various ro-vibrational states, on a recently calculated *ab initio* ground state potential energy surface. Both the wave packet and statistical quantum calculations were carried out within the centrifugal sudden approximation as well as using the exact Hamiltonian. Quantum reaction probabilities exhibit dense oscillatory pattern for smaller total angular momentum values, which is a signature of resonances in a complex forming mechanism for the title reaction. Significant differences, found between exact and approximate quantum reaction cross sections, highlight the importance of inclusion of Coriolis coupling in the calculations. Statistical results are in fairly good agreement with the exact quantum results, for ground ro-vibrational states of the reactant. Vibrational excitation greatly enhances the reaction cross sections, whereas rotational excitation has relatively small effect on the reaction. The nature of the reaction cross section curves is dependent on the initial vibrational state of the reactant and is typical of a late barrier type potential energy profile. © *2014 AIP Publishing LLC*. [http://dx.doi.org/10.1063/1.4895567]

I. INTRODUCTION

Understanding the dynamics of gas-phase bimolecular reactions has been one of the challenging areas of research, both experimentally and theoretically. Many direct and complex-forming atom-diatom scattering collisions have been studied in detail in an attempt to elucidate the underlying mechanisms which lead from reactants to products. Unlike in the direct reactions, the presence of deep potential wells and long-range electrostatic interaction in the asymptotic region of the corresponding potential energy surfaces (PES) in insertion reactions increases the complexity of these processes. Theoretical studies require, then, larger spatial grid sizes, making the quantum dynamical simulation computationally expensive.[1–13] Many of these systems possess no activation barrier in the entrance channel. As a result, a large number of partial waves is required to converge the cross sections and the *J*-shifting method usually does not work very well.[1,13,14] For the above reasons, the number of studies on reactions mediated by the formation of an intermediate species is far less compared to direct reactions.

Protonated rare gas species play an important role in interstellar and atmospheric chemistry and plasma physics. It is then not surprising that the structure and dynamics of, for example, RgH_2^+ (Rg = He, Ne, Ar) systems, have been the subject of a large number of both theoretical and experimental studies: *ab initio* electronic structure, ro-vibrational spectra, reaction cross sections, and rate constants have been calculated before.[4,6–8,15–26] Complexes containing two rare gas atoms and a proton are also well studied.[12,27–36] Both RgH_2^+ and $[RgHRg/Rg']^+$ cases are found to display a global potential energy minimum at the collinear configuration. Initial theoretical studies for systems with only one proton, H^+, concentrated on the determination of the stable electronic structure[27,29,30,35] and ro-vibrational energy states.[27,30,35] Quantum mechanical (QM) dynamical simulations have been carried out for the He + HeH^+ → HeH^+ + He reaction by some of us[33] using a time-dependent wave packet (TDWP) method within centrifugal sudden (CS) approximation, on a PES calculated at coupled-cluster singles and doubles with perturbative triples correction (CCSD(T))/aug-CC-PVTZ in 2003.[32] Later, CS and Coriolis coupled (CC) reaction probabilities for the same reaction were calculated by Xu and Zhang[12] on a recent surface computed by Liang *et al.*[34] The results in Ref. 12 show remarkable differences between the CS and CC approaches, in accordance with the results obtained for other ion-molecule systems.[7,8,10–12] Recently, we have explored the electronic structural details of $[RgHRg']^+$ (Rg = He, Ne, Ar)[35] type of systems.

In our previous work,[36] an analytical PES was generated for the $[HeHNe]^+$ system with a very small root mean square error and preliminary quantum dynamical studies were carried out for He + NeH^+ → HeH^+ + Ne reaction following a TDWP method within CS approximation. Dense oscillatory behavior of the reaction probabilities for this reaction indicated the involvement of an intermediate complex in the reactive process, a possibility also supported by the existence of a potential well with a depth of about 0.5 eV in the region between reactants and products. Whereas vibrational excitation of the reactant produced large enhancements in reactivity, the excitation of NeH^+ to first few rotational states was found to inhibit the reaction and further excitation to higher rotational states resulted in promoting the reactive process.

a)t.gonzalez.lezana@csic.es
b)adi07@iitg.ernet.in

It is well known that inclusion of CC is of paramount importance in atom-molecular ion systems as the CS approximated results differ from the exact results. The necessity of a proper treatment of the helicity components coupling in the bimolecular complex-forming scattering systems has been highlighted in many recent studies.[1,4,9,12,34,37–42] Keeping this in mind, we carry out here a CC versus CS comparative investigation by means of TDWP calculations for a better understanding of the $[HeHNe]^+$ process over the 0-0.5 eV collision energy range on the analytical PES of Ref. 36.

In order to test the above mentioned hypothesis of a complex-forming mechanism, we have also employed a statistical quantum mechanical (SQM) method to study the process. In particular, the approach developed in Refs. 43 and 44 has been successfully applied before to investigate many reactions.[45–51] The comparison of statistical predictions with TDWP reaction probabilities and cross sections will thus enable us to establish the relevance of this sort of mechanisms on the overall dynamics.

This paper is structured as follows: In Sec. II, details of the real wave packet (WP) and SQM methods are discussed. Results are presented in Sec. III, followed by conclusions in Sec. IV.

II. METHOD

A. Wave packet method

The quantum dynamical simulations for the title reaction were carried out by solving time-dependent Schrödinger equation on a grid using WPs. The Hamiltonian operator for $He + NeH^+$ system in reactant Jacobi coordinates is written as[52,53]

$$\hat{H} = -\frac{\hbar^2}{2\mu_R}\frac{\partial^2}{\partial R^2} - \frac{\hbar^2}{2\mu_r}\frac{\partial^2}{\partial r^2} + \frac{\mathbf{l}^2}{2\mu_R R^2} + \frac{\mathbf{j}^2}{2\mu_r r^2} + \mathbf{V}(R, r, \theta), \tag{1}$$

where R is the distance between He atom and the center of mass of NeH^+, r is the NeH^+ bond length, μ_R is the reduced mass of He and NeH^+, and μ_r is the reduced mass of NeH^+. Here, $\mathbf{l} = \mathbf{J} - \mathbf{j}$ is the orbital angular momentum operator. $\mathbf{J}$ and $\mathbf{j}$ are the total angular momentum and rotational angular momentum operators, respectively. $\mathbf{V}(R, r, \theta)$ is the interaction potential of the system.

The time-dependent wave function is expanded in terms of translational, vibrational, and body-fixed (BF) total angular momentum basis and is written in a mixed grid representation. A direct product discrete variable representation (DVR) for radial coordinates and a finite basis representation (FBR) for the angular coordinates are used. For the radial degrees of freedom, equidistant grids were defined whereas Gauss-Legendre quadrature points described the angular degrees of freedom. In this discrete grid representation, the Hamiltonian takes the shape of a tridiagonal matrix and is expressed as[52,54]

$$\begin{aligned}\hat{H} = \Bigg[&-\frac{\hbar^2}{2\mu_R}\frac{\partial^2}{\partial R^2} - \frac{\hbar^2}{2\mu_r}\frac{\partial^2}{\partial r^2} + \frac{j(j+1)}{2\mu_r r^2} \\ &+ \frac{J(J+1) + j(j+1) - 2K^2}{2\mu_R R^2} + V(R, r, \theta)\Bigg]\delta_{KK'} \\ &- \frac{\hbar^2}{2\mu_R R^2}\lambda^+_{JK}\lambda^+_{jK}\sqrt{1+\delta_{K0}}\,\delta_{K+1,K'} \\ &- \frac{\hbar^2}{2\mu_R R^2}\lambda^-_{JK}\lambda^-_{jK}\sqrt{1+\delta_{K1}}\,\delta_{K-1,K'},\end{aligned} \tag{2}$$

where λ is defined as $\lambda^{\pm}_{JK} = \sqrt{J(J+1) - K(K \pm 1)}$. Here, K is the projection of J on the body-fixed z-axis. Exclusion of the off-diagonal terms in Eq. (2) results in the CS approximation,[55,56] where K becomes a good quantum number and is taken as a constant. In CC calculations, this is not the case and the full expression in Eq. (2) is used, though for most of the cases the maximum value of K (K_{max}) converges to a comparatively smaller number. In this work, we have carried out both CS and CC calculations for the title reaction. Our quantum dynamics CC code is parallelized over the K states using message passing interface (MPI) library. Shared memory parallelization technique is applied to both the CS and CC codes to decrease the time factor by using OPENMP library.

The WP is propagated by following the Chebyshev real wave packet method.[2,3,57] The Chebyshev operator is simply a cosine propagator and can be imagined as the real part of the exponential time evolution operator.[58–61] In this case, the Hamiltonian is normalized to $[-1,1]$[58,59] by introducing a scaled Hamiltonian ($\hat{H}_s$) which is represented as

$$\hat{H}_s = (\hat{H} - H^+)/H^-, \tag{3}$$

where $H^+ = (H_{max} + H_{min})/2$ and $H^- = (H_{max} - H_{min})/2$. Here, H_{max} and H_{min} are the upper and the lower bounds of the eigenvalues of the Hamiltonian, respectively.

The Chebyshev propagator follows the modified recursion relation[62]

$$\Phi_{k+1} = D(2\hat{H}_s\Phi_k - D\Phi_{k-1}), \tag{4}$$

where $\Phi_0 = \Psi(R, r, \theta, t = 0)$, the initial WP and $\Phi_1 = D\hat{H}_s\Phi_0$. A Gaussian shaped damping wave function (D) is used to damp the WP near the end of the grid to avoid unphysical reflection from grid end. Here, the following form of D is used:

$$D = \begin{cases} \mathrm{Exp}(-\mathrm{A_x}(\mathrm{x} - \mathrm{x_d})^2), & \text{for } x > x_d, \\ 1 & \text{elsewhere,} \end{cases} \tag{5}$$

where A_x is the damping coefficient, x the coordinate along which the damping function is applied, and x_d is the starting point of damping.

In the CS calculations, the initial WP is prepared for a particular vibrational (v_0), rotational (j_0), total angular momentum (J) state in BF representation, and is written as follows:

$$\Psi_{v_0 j_0 J}(R, r, \theta, t = 0) = G_{k_0}(R)\,\phi_{v_0 j_0}(r)\,\widetilde{P}_{j_0 K}(\cos\theta). \tag{6}$$

$G_{k_0}(R)$ is a real Gaussian WP representing the relative translational motion of the system and is expressed as[3,57]

$$G_{k_0}(R) = N\exp(-(R - R_0)^2/2\delta^2)\cos(k_0 R), \tag{7}$$

where R_0 is the location of the center of the WP, δ is the width parameter, k_0 is the momentum wave vector, and N is

the normalization constant of the WP. $\phi_{v_0 j_0}(r)$ are the rovibrational eigenfunctions of NeH^+ and are computed by following the Colbert-Miller[63] approach. $\widetilde{P}_{j_0 K}(\cos\theta)$, the normalized associated Legendre polynomials, are the eigenfunctions of $\mathbf{j}^2$ operator and are written as

$$\widetilde{P}_{j_0 K}(\cos\theta) = \sqrt{\frac{(2j_0+1)}{2}\frac{(j_0-K)!}{(j_0+K)!}} P_{j_0 K}(\cos\theta). \quad (8)$$

Preparation of the initial WP is a bit different for the CC calculations. At first, the initial WP is prepared in the space fixed (SF) representation for a particular v_0, j_0, and l_0 state and is written as

$$\Psi^{JMp}_{v_0 j_0 l_0}(R, r, \theta, t=0) = G_{k_0}(R)\,\phi_{v_0 j_0}(r)\,|JMj_0 l_0 p\rangle, \quad (9)$$

where $|JMj_0 l_0 p\rangle$ is the parity-adapted total angular momentum eigenfunction with p being the parity of the system and M is the projection of J on the SF z-axis. The initial orbital angular momentum quantum number l_0 lies between $|J - j_0|$ and $J + j_0$, for a given J and j_0. Since the propagation is carried out in BF representation, the initial l_0-dependent WP state is transformed into the corresponding K-dependent wave function in BF representation as[53,64,65]

$$|JMj_0 l_0 p\rangle = \sum_{K\geq 0} C^{j_0 Jp}_{l_0 K}\,|JMj_0 K\rangle. \quad (10)$$

Here, $C^{j_0 Jp}_{l_0 K}$ is the transformation matrix between the two representations given by

$$C^{j_0 Jp}_{l_0 K} = \sqrt{\frac{(2l_0+1)}{2J+1}}\sqrt{(2-\delta_{K,0})}\,\langle j_0 K l_0 0|JK\rangle, \quad (11)$$

where $\langle j_0 K l_0 0|JK\rangle$ is the Clebsch-Gordan coefficient.

During the propagation, the action of radial kinetic energy operator is evaluated using the fast Fourier transform (FFT) approach while the evaluation of action of the angular momentum operator on the WP is performed in associated Legendre polynomial basis set. At first, the WP is transformed through a DVR transformation by multiplying it with

$$T^K_{nj} = \sqrt{w_n}\,\widetilde{P}_{jK}(\cos\theta_n), \quad (12)$$

where n denotes the index of the quadrature points and w_n is the corresponding weight. The action of the angular momentum operator in Eq. (2) is carried out in local representation on this transformed WP and the final expression is obtained by transforming back to the DVR basis.

As R approaches zero, matrix elements of the local angular momentum operators become very large and the CC calculations become unmanageable. To get rid of this problem, the recipe proposed by Zanchet *et al.*[66] is followed. In this formulation, a particular value of R, R_{cut}, is chosen for a particular J. At $R = R_{cut}$, the average value of the matrix elements of $\mathbf{l}^2$ operator in Eq. (2) is equal to a given E_{cut} (E_{cut} is a sufficiently high constant energy value[2,3]). In the calculations, $R < R_{cut}$ are replaced by R_{cut}.

The energy-dependent total reaction probability is computed by summing the total flux of the energy dependent WP going through a fixed surface located at sufficiently large distance (r_s) in the product channel,[57,65,67]

$$P^r(E) = \frac{1}{2\pi\mu_r |a_i(E)^2|(H^-)^2\sin^2\Theta} \times \mathrm{Im}\left\langle \sum_k (2-\delta_{k0})\,\mathrm{Exp}(-ik\Theta)\,\Phi_k \left| \sum_{k'} (2-\delta_{k'0})\,\mathrm{Exp}(-ik'\Theta) \times \left[\delta(r-r_s)\frac{\delta}{\delta r}\Phi_{k'}\right]\right\rangle. \quad (13)$$

Here, $\cos\Theta = (E - H^+)/H^-$ and a_E is the energy weightage of the initial translational WP and is expressed as[2,3,68]

$$a_i(E) = \left\langle i\sqrt{\frac{\mu_R k_i}{2\pi}} R h^{(2)}_l(k_i R)|G_{k_0}(R)\right\rangle. \quad (14)$$

Here, $h^{(2)}_{l_0}$ is the spherical Hankel function of the 2nd kind and $k_i = \sqrt{2\mu_R E_c}/\hbar^2$. Use of Hankel function helps us to place the initial WP at small R where the interaction potential $V \to 0$. In the CS calculations for $j_0 > 0$, l_0 was approximated to the nearest integer root for l_0 of the relation $l_0(l_0 + 1) = J(J+1) + j_0(j_0+1) - 2K^2$.[69] For the CC calculations, the J-dependent total reaction probabilities were calculated by averaging over all possible l_0-dependent total reaction probabilities.[2]

The total reaction cross section is obtained from the J-dependent probabilities using the following formula:

$$\sigma_{v_0 j_0}(E) = \frac{\pi}{k^2_{v_0 j_0}} \sum_{J=0}^{J_{max}} (2J+1) P^J_{v_0 j_0}(E_c), \quad (15)$$

where $k_{v_0 j_0}$ is the wave number corresponding to the initial state at a fixed collision energy E_c.

B. Statistical quantum method

The SQM was originally designed to treat complex-forming atom-diatom reactions.[43–45] Under the assumption that the collision proceeds via the formation of an intermediate complex between reactant and products, it is possible to write the reaction probability for the initial rovibrational state v_0, j_0 and the J total angular momentum as

$$P^J_{v_0 j_0}(E_c) \simeq \frac{p^J_{v_0 j_0}(E_c)\sum_{v'j'} p^J_{v'j'}(E_c)}{\sum_{v''j''} p^J_{v''j''}(E_c)}, \quad (16)$$

where $p^J_{v_0 j_0}$ corresponds to the capture probability for the complex to be formed starting from the $NeH^+(v_0, j_0)$ initial rovibrational state and $p^J_{v'j'}$ to the individual probability for the complex to fragment into the $HeH^+(v', j')$ state. The sum in the denominator runs over all energetically open states in both reactant and product channels. The corresponding cross sections are then calculated by introducing probabilities from Eq. (16) into the above expression (15).

The capture probabilities p^J_{vj} are computed by solving a set of close-coupled equations for each arrangement with the form

$$\Psi'' = W(R)\Psi(R), \quad (17)$$

where the interaction matrix $W(R)$ is expressed as

$$W^J_{v'j'l',vjl}(R) = \left[\frac{2\mu}{\hbar^2}(E_{vj} - E) + \frac{l(l+1)}{R^2}\right]\delta_{v'v}\delta_{j'j}\delta_{l'l} + \frac{2\mu}{\hbar^2}V^J_{v'j'l',vjl}(R), \quad (18)$$

μ being the three-body reduced collision mass in order to express the Hamiltonian in mass-reduced coordinates[70] and l the orbital angular momentum quantum number. The interaction potential matrix $V^J_{v'j'l',vjl}$ can be finally expressed in terms of the diatomic vibrational wavefunctions, vector-coupling coefficients, and spherical harmonics.[43]

The equations of expression (17) are solved after a transformation into a Ricatti equation[43] and a log-derivative propagation[71] between certain capture radius $R_{\min}$ at which the intermediate complex is formed and $R_{\max}$ which defines the asymptotic region. The values for such distances employed in this work are, for the He+NeH$^+$ reactant channel: $R_{\min} = 4.4$ a$_0$ and $R_{\max} = 10.2$ a$_0$; and for the HeH$^+$ +Ne product channel: $R_{\min} = 4.0$ a$_0$ and $R_{\max} = 8.0$ a$_0$.

Besides the CC scheme described in Eq. (18) it is also possible to perform the SQM calculation within the CS approximation. In this approach, a smaller set of coupled-channel equations for each value of K, the projection of the angular momentum on the atom-diatom axis, is obtained

$$W^{JK}_{v'j',vj}(R) = \left[\frac{2\mu}{\hbar^2}(E_{vj} - E) + \frac{l(l+1)}{R^2}\right]\delta_{v'v}\delta_{j'j} + \frac{2\mu}{\hbar^2}V^K_{v'j',vj}(R), \quad (19)$$

where

$$l = [J(J+1) + j(j+1) - 2K^2 + 1/4]^{1/2} - 1/2. \quad (20)$$

The SQM calculations have been performed with a maximum value of the energy of 1.2 eV thus allowing up to $v_{\max} = 3$ and $j_{\max} = 23$ as the largest values of the vibrational and rotational quantum numbers, respectively, for the reactant arrangement and $v'_{\max} = 2$ and $j'_{\max} = 14$ for the products at $E_c = 0.5$ eV, the highest collision energy considered in this study.

III. RESULTS AND DISCUSSION

A. Probabilities and opacity functions

As mentioned already, the analytical surface recently computed by us has been used for dynamical calculations. More than 19 000 *ab initio* (CCSD(T)/aug-cc-pVQZ) energies of [HeHNe]$^+$ were fitted to Aguado-Paniagua many body expansion functions[72] with a root mean square error less than 0.03 kcal/mol. A schematic potential energy profile of reactants, products, and the minimum is shown in Figure 1. Some selective reactants and products ro-vibrational states are also depicted in the same picture. It is clear from the figure that the title reaction is endothermic by 0.293 eV with reactants in the ground ro-vibrational states, but vibrational excitation of the reactant makes the process exothermic. As shown in Figure 1, there exists a potential energy well of depth 0.521 eV along the minimum energy path.

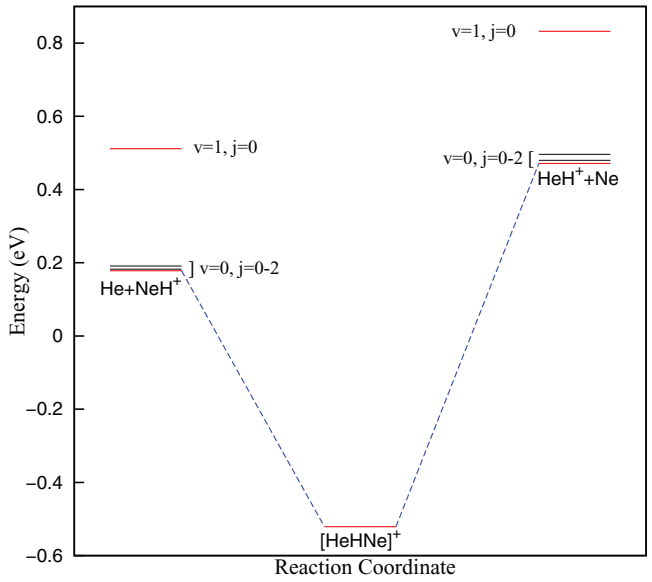

FIG. 1. Schematic potential energy profile of reactants and products for the title reaction.

All the QM results reported here were computed by following Chebyshev real WP propagation method. Here, it is worth mentioning that the present QM-CS results are in excellent agreement with our previous QM-CS results[36] when the previous probabilities are modified with an energy distribution calculated using spherical Hankel functions, as in the present case. The parameters used in the QM calculations are given in Table I. The reaction probabilities were calculated in the collision energy range of 0.0-0.5 eV with an energy resolution of 0.0005 eV. For $v_0 = 0$, the maximum values of J ($J_{\max}$) are 67 and 74 for QM-CS and QM-CC calculation, respectively, while for $v_0 = 1$, $J_{\max} = 91$ was enough for both the QM-CS and QM-CC calculations to converge the integral cross sections (ICSs) within the above energy range.

In Figure 2, the convergence of the QM-CC reaction probabilities with respect to $K_{\max}$ (maximum value of K) is shown for different initial reactant states at large J values. For $v_0 = 0$ and 1, $J = 50$ and 70 are chosen to investigate the $K_{\max}$ dependence on total reaction probabilities. As can be seen in Figures 2(a) and 2(b), there are very small differences between the reaction probabilities for $K_{\max} = 7$ and 11.

TABLE I. Parameters used in the dynamical simulations (all parameters are given in atomic units).

Number of R grid points	220
Number of r grid points	150
Number of angular grid points	120
R_{min}	0.2
r_{min}	0.5
δR	0.1
δr	0.12
Center of initial wave packet	14.0
Damping coefficients along R and r	0.001, 0.001
Starting points of damping along R and r	15.5, 13.22
Analysis point along r	12.98
Number of Chebyshev iterations	30 000

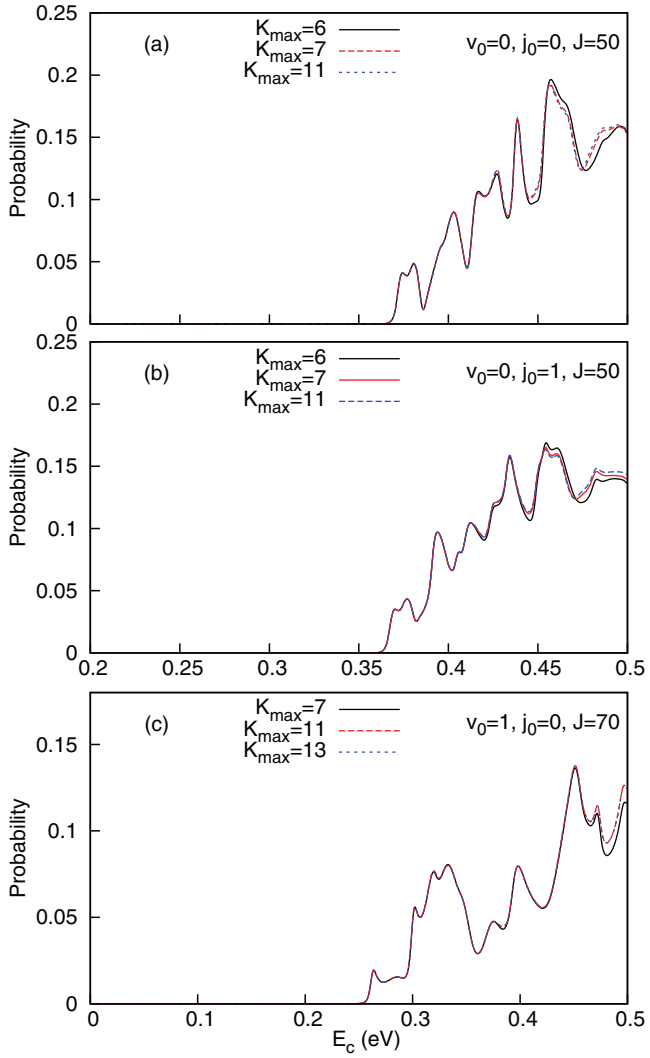

FIG. 2. Dependence of reaction probabilities on K_{max} (maximum number of K used). (a)–(c) Results are shown for three different initial states and for two different J values.

Considering the computational cost and time factor as well as accuracy of the calculations, $K_{max} = \min(J, 7)$ were used for all $v_0 = 0$ calculations. However, for $v_0 = 1$ a large number of J's were needed to converge the cross sections within the investigated energy range. As it is observed in Figure 2(c), $K_{max} = 11$ calculation slightly overestimates the reaction probability compared to $K_{max} = 7$, but reaction probabilities obtained by using $K_{max} = 11$ and 13 are same. In this case, $K_{max} = 11$ was used for $J > 50$ calculations and $K_{max} = \min(J, 7)$ were used in rest of the calculations.

Different initial-state selected QM and SQM total reaction probabilities for the title reaction, for some selective J's, are plotted in Figure 3. Both the QM-CC and QM-CS probabilities exhibit dense oscillations for low J values, which may be an indication of an intermediate complex getting formed in the deep potential well during the reaction. Such dense oscillatory total reaction probabilities have been seen for many other bimolecular complex forming reactions.[1–9,11,12,25,33,73,74] For larger J values, the peaks in the probability curves become broader. The other significant observation is that the amplitude of the oscillations are larger for the CS probabilities than those in the CC results. CC probability for a particular value of J is calculated by summing over the probabilities of all the individual K states included in the CC calculation. As a result, the resonance features of the individual K-dependent probabilities are diminished in the resultant CC probabilities. As it is seen in Figure 3, the reaction has a threshold of ~0.29 eV for ground ro-vibrational state of the reactants and the threshold increases for higher J values due to the increase of centrifugal barrier. For $v_0 = 0$ reactions, the QM-CC probabilities for larger J values (e.g., $J = 50$, 60) have smaller threshold energies than the corresponding thresholds in QM-CS probabilities. The N_K-dependent effective potential energy profiles, plotted in Figure 4, address this difference. Here, N_K is number of K states included in QM-CC calculations. The effective potential energies ($E(R, r)$) for a particular J and N_K are calculated as

$$E(R, r) = F/2\mu_R R^2 + V(R, r), \tag{21}$$

where F is the smallest eigenvalue obtained by diagonalizing the centrifugal tridiagonal matrix of Eq. (2) and $V(R, r)$ are the potential energies of the system along the collinear minimum energy path. As the angular kinetic energy decreases with the increase in K (see Eq. (2)), the term F, described in Eq. (21) also decreases. This results in a lower effective

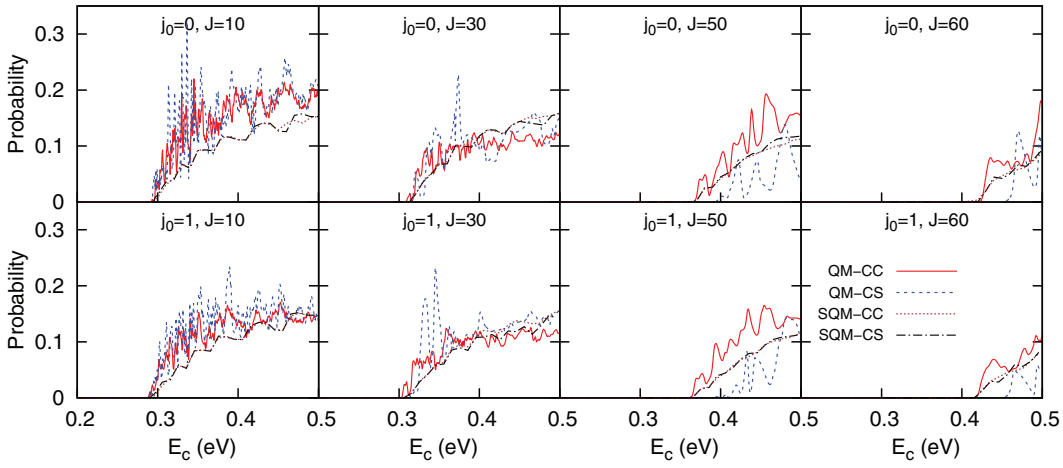

FIG. 3. Total reaction probability plotted as a function of collision energy (E_c) for $v_0 = 0, j_0 = 0$ and 1, for different J values.

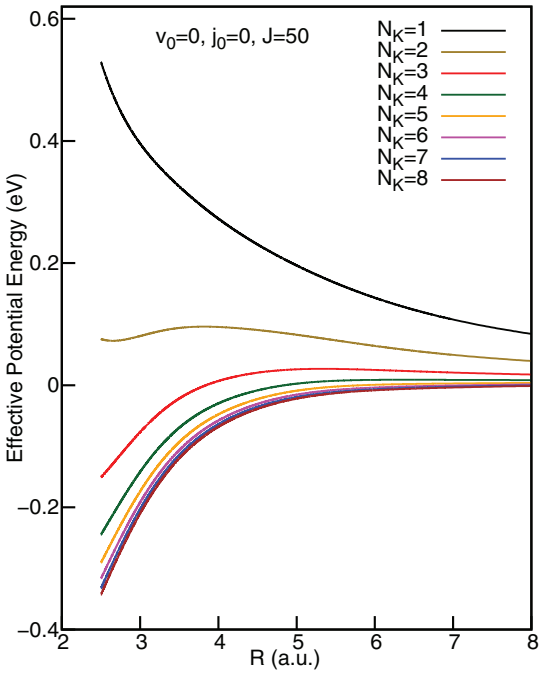

FIG. 4. Effective potential energy profiles for the He+NeH$^+$ reaction at $J = 50$. Horizontal axis corresponds to the collinear minimum energy path. N_k is the number of K states used.

potential energy. Thus, more the number of K states included in the QM-CC calculations, less is the value of the effective potential energy and this feature is reflected in Figure 4. In CS calculations, on the other hand, N_K is always equal to one and the centrifugal barrier is independent of N_K.

In Figure 3, the similarities between QM-CC and QM-CS reaction probabilities for low J values ($J = 10$) are quite clear but differences increase with the increase of total angular momentum. These findings are in accordance with the results for other atom-molecular ion systems[4,8,11] for which it has been observed that Coriolis coupling becomes more important as the value of J increases. The contributions of each K state to the total QM-CC reaction probabilities for $v_0 = 0, j_0 = 0$, 1, and $J = 10$, 40 are presented in Figure 5. It is obvious from this figure that for $v_0 = 0, j_0 = 0$, 1, and $J = 10$, the major part of the reaction probabilities comes from first three K states and the contributions are negligibly small from large K states. However, for $J = 40$, the initial WP is channeled to larger K states to overcome the centrifugal barrier and more number K states contribute significantly to the reaction probabilities. In the CS calculations, the out of plane rotations of molecule are restricted and only one K state (here $K = 0$) is included during quantum calculations. As a result, it can be seen in Figure 3 that there are no significant differences between the QM-CS and QM-CC reaction probabilities for $v_0 = 0, j_0 = 0$, and $J = 10$, where major share of the QM-CC reaction probabilities comes from $K = 0$ state. However, it is found that the differences between QM-CS and QM-CC reaction probabilities increase a bit for $v_0 = 0, j_0 = 1$, and $J = 10$, where $K = 0$ and 1 states have almost similar contribution to the total QM-CC reaction probability.

Figure 3 also shows the SQM probabilities and the effect of rotational excitation on the reaction attributes. For $v_0 = 0$, all the QM and SQM reaction probabilities have thresholds and the probabilities gradually increase with the increase of collision energy, which is in accordance with many other endothermic reactions.[4–7,11,25,73] The rotational excitation of the reactants to its first excited state has less effect on the reaction probabilities. It is found that the reaction probabilities for $j_0 = 1$ are very much comparable to the corresponding $j_0 = 0$ probabilities near the threshold regions, but at higher collision energy $j_0 = 1$ probabilities are slightly smaller than the

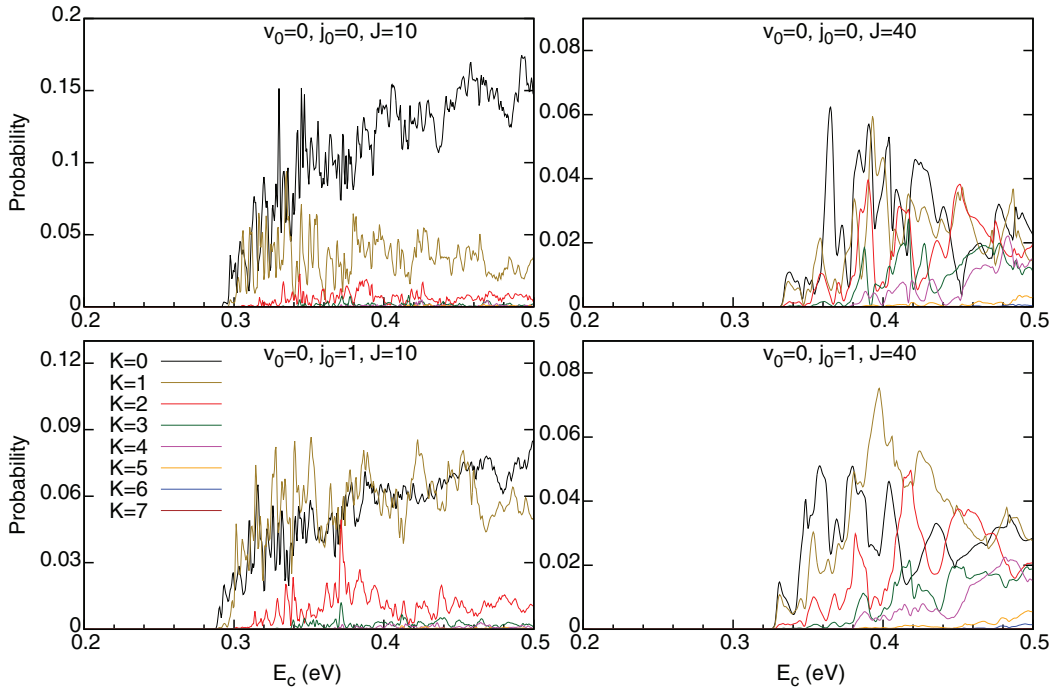

FIG. 5. K-dependent total reaction probabilities for different combinations of ro-vibrational and J states, as shown in the figure.

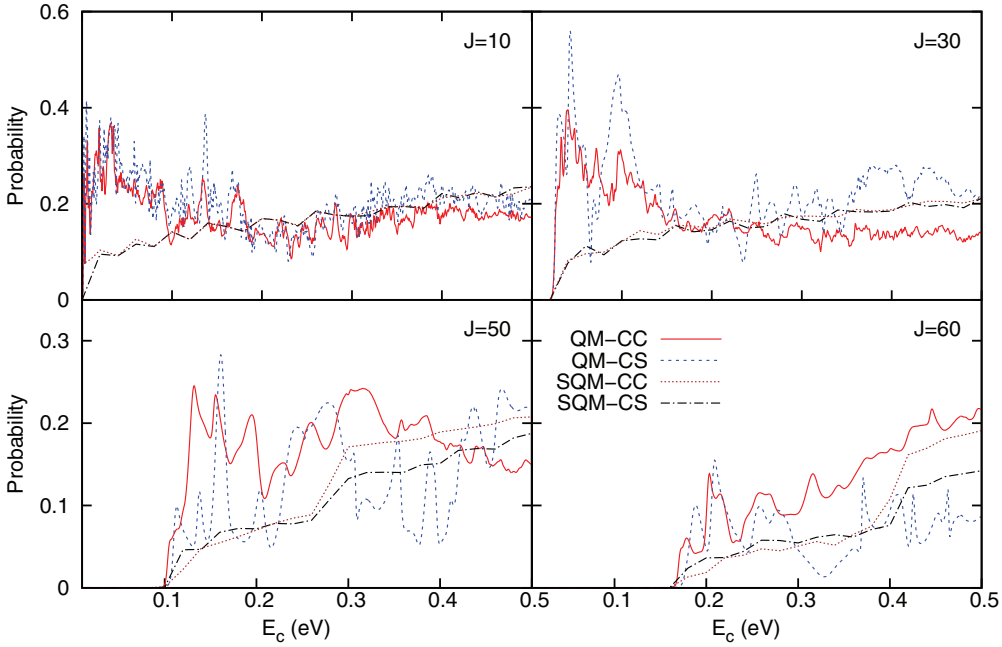

FIG. 6. Total reaction probability plotted as a function of collision energy (E_c) for $v_0 = 1, j_0 = 0$, for different J values.

$j_0 = 0$ probabilities. A small increase in reactant energy due to rotational excitation is not sufficient to compete with the steric preference (collinear) for the reaction. The SQM results for $v_0 = 0$ produces a fairly good description of the process, when compared with the QM-CC results. Although the statistical predictions account for the overall trend of the TDWP probabilities, the resonance structure cannot be reproduced, a consequence of the approximation assumed in Eq. (16) which neglects any information regarding the phase of the scattering matrix.

For $j_0 = 0$ and $J = 10$, the SQM results start being almost the same as the QM probabilities, but when the collision energy is increased, they start to differ and remain smaller over the rest of the collision energies. For $v_0 = j_0 = 0$, $J = 30$, and E_c beyond 0.4 eV, the SQM method produces probabilities which are slightly larger than the QM-CC results. For $J = 50$, the trend reverses and SQM results are smaller than the QM-CC results over the 0.4-0.5 eV energy range. For $j_0 = 1$ and $J = 10$ and 30, SQM predictions are almost in the same range as QM-CC results. For $J = 50$ and 60, the SQM probabilities are generally smaller than the QM-CC values.

The effect of vibrational excitation of the reactant is shown in Figure 6. As is seen in Figure 1, vibrational excitation makes the reaction thermodynamically exothermic, which results in a strong enhancement in the reaction probabilities. For $v_0 = 1$, the reaction probabilities for lower J values start without any threshold, which is typical for barrierless exothermic reactions[2,3,8,9,74] and processes with reactants in vibrationally excited states.[5–7,12,25,81] For $J = 10$, the SQM results are very small compared to the QM results in 0.0-0.1 eV energy range. In the rest of the regions, the statistical method shows a very good agreement with the QM results. For $J = 30$, despite the good description of the reaction thresholds, the SQM probabilities are again much smaller than the QM results in 0.0-0.15 eV energy region. Beyond 0.35 eV, those are slightly larger than QM-CC results. For other larger J values, the probabilities produced by SQM are smaller than the QM results over almost the whole energy range.

Surprisingly, both the SQM-CS and SQM-CC reaction probabilities behave similarly with the only exception of the results at the large values of the energy (beyond 0.3 eV for $J = 50$ and 0.4 eV for $J = 60$), being the CC probabilities slightly larger than the SQM-CS values, as observed for the TDWP calculation especially for $J = 60$. The situation thus differs, for instance, with reported results for the H_3^+ reaction.[75] For this process and the corresponding isotopic variants, CS and Coriolis decoupling schemes have been found to introduce noticeable deficiencies.[37,76,77] In particular within the SQM framework, the CS approximation was responsible for the differences observed for opacity functions $P^J(E)$ with respect to both exact QM results[78] and predictions obtained by means of a quasiclassical trajectory version of the SQM approach (SQCT).[79,80] It is worth noticing however that these discrepancies between SQM-CC and SQM-CS results were more relevant at the state-to-state level.

The apparent failure of the SQM approach to account for the behavior at the lower energy regime displayed by the TDWP probabilities for the reaction initiated from $NeH^+(v_0 = 1, j_0 = 0)$ seems to be related with the dependence observed with R_{min}, the capture radius employed in the log-derivative propagation. While this feature does not constitute an issue for the $NeH^+(v_0 = 0, j_0 = 0)$ case, no proper convergence of the probabilities, $P^J_{v_0=1,j_0=0}(E)$ with respect to R_{min} was achieved. A possible explanation could be the different topology of the PES of Ref. 36 depending on the value of Ne–H–He angle. Thus, whereas the minimum is observed for the 180° collinear approach, a remarkable barrier in the minimum energy path is found for 90° (see Fig. 2 of Ref. 36). It might occur then that the chosen R_{min} is valid for specific

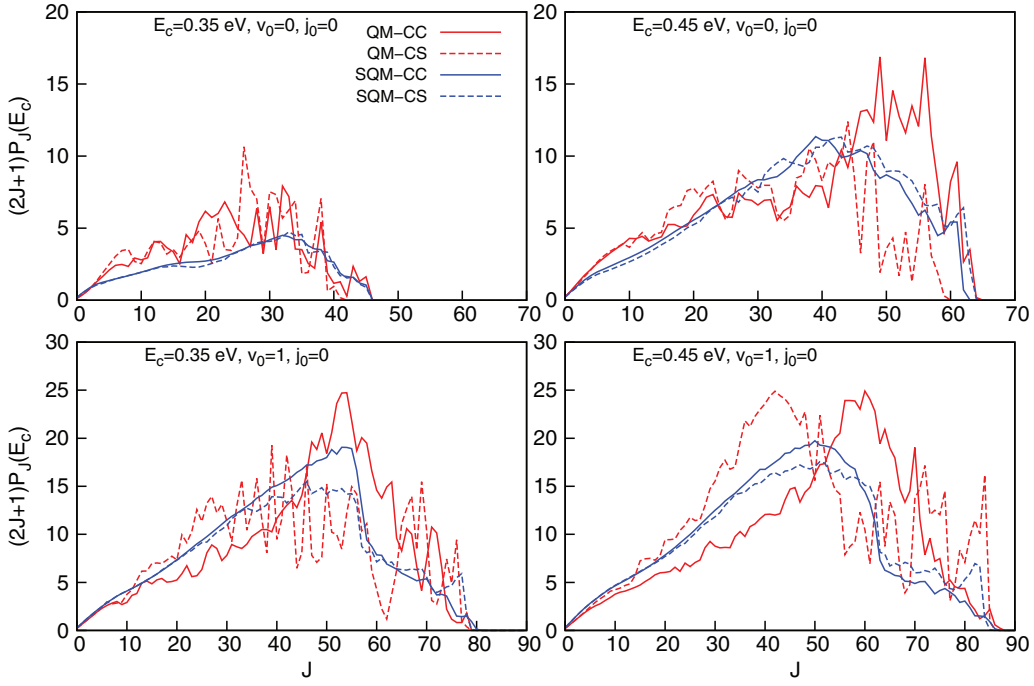

FIG. 7. Partial waves contributions to the total integral cross sections plotted as a function of total angular momentum for the title reaction for $v_0 = 0$, 1 and $j_0 = 0$ reactant states, at different collision energies as mentioned.

geometries but some refinement should be considered for different approaching angles. Present work in progress considers more flexible definitions for such capture radius. In this sense, it is worth pointing out the scheme based on energy considerations to stop the propagation of the quasiclassical trajectories performed in the above mentioned SQCT method.[79,80]

Another reason for the observed deviations at low energies of the SQM predictions with respect to the TDWP results could be the depth of the potential, 0.5 eV, perhaps insufficiently large to guarantee a complete description of the dynamics on statistical grounds. The present case, He+NeH$^+$, differs in this sense, with processes mediated by a complex-forming pathway, for example, S(^1D)+H_2, C(^1D)+H_2, N(^2D)+H_2, or O(^1D)+H_2,[44,45] with minima of 4.23, 4.29, 5.48, and 7.29 eV deep, respectively. For this sort of reactions, the SQM approach reproduced most of the main dynamical features.

The opacity functions, reaction probabilities as a function J at particular collision energies, are plotted as $(2J+1)P^J(E_c)$ in Figure 7. There are significant differences between QM-CC and QM-CS results, while both the SQM-CC and SQM-CS results are almost identical. For $v_0 = 0$, the results obtained by the SQM approach show a good average description of the quantum mechanical results. For $v_0 = 1$, the maximum of the curve shifts to larger J values compared to the QM-CS ones. In this case, smaller J's contribute more to the total cross sections for QM-CS than for QM-CC calculations, while larger J values contribute more to QM-CC results.

The SQM probabilities for the reaction initiated in the vibrationally excited NeH$^+$($v_0 = 1$), almost the same for both the CC and CS cases, seem to reproduce the existing decrease in the values of $(2J+1)P^J(E_c)$ for $J \sim 60$ displayed by the QM-CS result.

B. Integral cross sections

The total ICSs calculated by QM and SQM approaches are plotted in Figure 8, for different reactant ro-vibrational states. The resonances observed in QM reaction probabilities are mostly diminished in the cross section curves due to J-averaging effect. The cross sections for $v_0 = 0$ increase steadily within the investigated energy range, as is the case for other endothermic reactions. QM-CC ICSs for $v_0 = 0$ and $j_0 = 0$, 1 are a bit smaller than the results obtained using QM-CS around the threshold region but are considerably larger than the QM-CS ones at higher collision energies. It was reported in our previous study[36] that the collinear path is the most preferable path for the He + NeH$^+$ reaction at low collision energies. In the CS calculations, there are more chances for head-on collisions between the reactants and this results in larger QM-CS cross sections near threshold regions. Coriolis coupling between different K-states opens up more dissociation channels for the complex to break and form the products. This leads to larger cross sections in case of QM-CC than the results in QM-CS.[4,8,10] Thus, at higher collision energies Coriolis coupling effect promotes the reactivity for the title reaction.

Figure 8 also shows the effect of rotational and vibrational excitation on the cross sections. No significant differences are observed in the cross sections between the $v_0 = 0$, $j_0 = 0$ and $v_0 = 0$, $j_0 = 1$ results below 0.45 eV of collision energy. Beyond this energy, differences are seen to increase. Similar trends were observed in case of He + H_2^+ reaction cross sections.[6] The reaction cross sections for $v_0 = 1$, $j_0 = 0$ are very high at low collision energies and the magnitude decreases sharply with the increase in collision energy and remains almost constant with further increase in

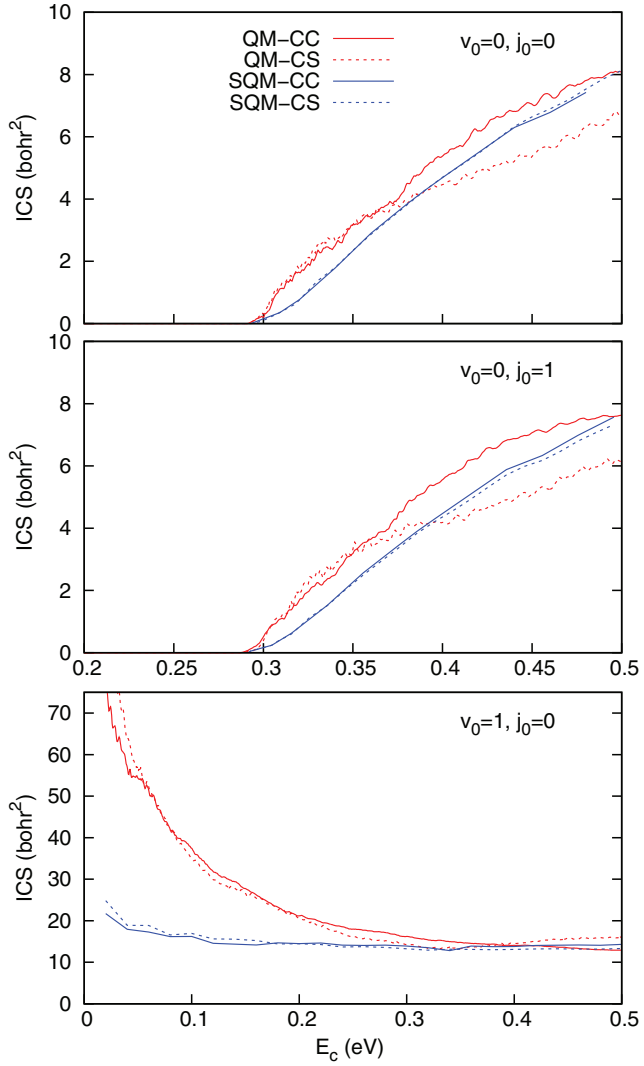

FIG. 8. Total integral reaction cross sections for He + NeH^+ ($v_0 = 0$, 1 and $j_0 = 0$, 1) → HeH^+ + Ne reaction. Both the QM and SQM results are presented.

collision energy. Similar observations were reported for other barrierless exothermic processes[8,9,74] and for reactions with reactants in their vibrationally excited states in late barrier type surfaces.[5–7,81] In the present system, the barrier corresponds to the reaction endothermicity. As suggested before in the case of the reaction probabilities, the cross sections obtained by means of the SQM method do not vary substantially when either the CC or CS framework is adopted: No significant differences are observed in SQM results shown in the three cases of Fig. 8 in the entire energy range under study. For $v_0 = 0$ (see top and middle panels of Fig. 8), the statistical cross sections remain below the QM-CC results up to the highest energy $E_c = 0.5$ eV, and crosses the QM-CS cross sections around $E_c \sim 0.38$ eV.

The most remarkable feature however is observed for the $v_0 = 1$ case (see bottom panel of Fig. 8) at the low energy region. The statistical cross sections clearly underestimate the TDWP values in consistency with our results for reaction probabilities (see Fig. 6). It is worth mentioning that barrierless processes yielding decreasing cross sections as the

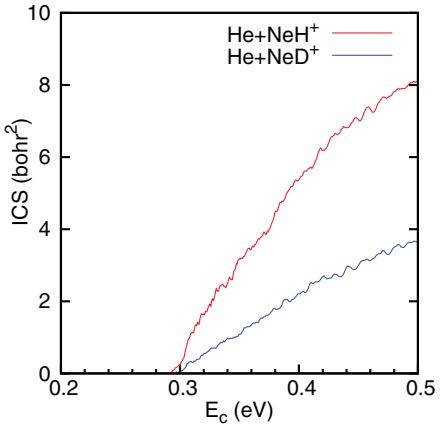

FIG. 9. Comparison of CC total cross sections for He + NeH^+ ($v_0 = 0, j_0 = 0$) → HeH^+ + Ne and He + NeD^+ ($v_0 = 0, j_0 = 0$) → HeD^+ + Ne reactions.

energy increases have been successfully studied before with the present SQM approach. In cases such as $C(^3P)$+OH → + H[49] or $O(^1D)$+H_2 → OH+H,[82] the statistical predictions reproduced correctly both QM and experimental cross sections. In Sec. III A, we discussed about the possible origin for the observed SQM failure for the He+NeH^+($v_0 = 1$, $j_0 = 0$) reaction.

Figure 9 shows the effect of isotopic substitution in the reactants on QM-CC reaction cross sections for the title reaction in its ground ro-vibrational state. It is observed that although both the total reaction cross section curves follow the same trend, the reaction cross sections for He + NeD^+ reaction are almost half of those for He + NeH^+ reaction. Interaction in NeD^+ molecule is stronger than in NeH^+ molecule. A weaker bond in NeH^+ gets more easily dissociated than the bond in NeD^+, leading to a very large cross section over all the energy range.

IV. CONCLUSIONS

In this work, a real WP method and SQM method have been applied to study the He + NeH^+ reaction for different reactant ro-vibrational states, on the ground electronic state. QM-CC and QM-CS reaction probabilities are close to each other for smaller J values, but significant differences are observed between the two sets of results as value of J increases. For $v_0 = 0$, QM-CC reaction cross sections are larger than the QM-CS ones at higher energies. The discrepancies between the QM-CC and QM-CS reaction cross sections for $v_0 = 1$ are also noticeable. These observations indicate the importance of inclusion of Coriolis coupling in the quantum mechanical studies for the title reaction. No remarkable disagreement are observed between the SQM-CC and SQM-CS reaction probabilities. The statistical method largely reproduces the trend of the quantum results, but integral cross sections underestimate the QM results for $v_0 = 0$. The reasonable agreement observed between the WP and SQM methods suggests the role played by a complex-forming mechanism for the present reaction. In fact, the statistical approach thus constitutes a valuable alternative to probe the dynamics of more complex reactions for which exact QM calculations turn out

computationally too expensive. Examples of these situations have been found in the past for $Si+O_2 \rightarrow SiO+O$.[51]

ACKNOWLEDGMENTS

This study was supported in part by a research grant from the Department of Science and Technology, New Delhi, India (DST Project No. SB/S1/PC-035/2013) and Project No. FIS2011-29596-C02-01 of the Spanish MICINN. We acknowledge the Center for Development of Advance Computing (CDAC), Pune, for providing us the high performance computing facility. L.B. also thanks support from Spanish MEC under Project No. COOPA20039.

[1]H. Guo, Int. Rev. Phys. Chem. **31**, 1 (2012).
[2]S. Y. Lin and H. Guo, J. Phys. Chem. A **108**, 2141 (2004).
[3]S. Y. Lin and H. Guo, Phys. Rev. A **74**, 022703 (2006).
[4]S.-J. Lv, P.-Y. Zhang, K.-L. Han, and G.-Z. He, J. Chem. Phys. **132**, 014303 (2010).
[5]L. González-Sánchez, O. Vasyutinskii, A. Zanchet, C. Sanz-Sanz, and O. Roncero, Phys. Chem. Chem. Phys. **13**, 13656 (2011).
[6]D. D. Fazio, M. D. Castro-Vitores, A. Aguado, V. Aquilanti, and S. Cavalli, J. Chem. Phys. **137**, 244306 (2012).
[7]P. Gamallo, P. Defazio, and M. González, J. Phys. Chem. A **115**, 11525 (2011).
[8]M. Hu, W. Xu, X. Liu, R. Tan, and H. Li, J. Chem. Phys. **138**, 174305 (2013).
[9]W. Xu, W. Li, S. Lv, H. Zhai, Z. Duan, and P. Zhang, J. Phys. Chem. A **116**, 10882 (2012).
[10]J. Zhao and Y. Luo, J. Phys. Chem. A **116**, 2388 (2012).
[11]E. Aslan, N. Bulut, J. F. Castillo, L. Bañares, O. Roncero, and F. J. Aoiz, J. Phys. Chem. A **116**, 132 (2012).
[12]W. Xu and P. Zhang, J. Phys. Chem. A **117**, 1406 (2013).
[13]H. Yang, K.-L. Han, G. C. Schatz, S. C. Smith, and M. Hankel, Phys. Chem. Chem. Phys. **12**, 12711 (2010).
[14]H. Yang, K.-L. Han, G. C. Schatz, S. H. Lee, K. Liu, S. C. Smith, and M. Hankel, Phys. Chem. Chem. Phys. **11**, 11587 (2009).
[15]P. Palmieri, C. Puzzarini, V. Aquilanti, G. Capecchi, S. Cavalli, D. De Fazio, A. Aguilar, X. Gimenez, and J. M. Lucas, Mol. Phys. **98**, 1835 (2000).
[16]B. Maiti, C. Kalyanaraman, A. N. Panda, and N. Sathyamurthy, J. Chem. Phys. **117**, 9719 (2002).
[17]T. Zhang, X.-M. Qian, X. N. Tang, C. Y. Ng, Y. Chiu, D. J. Levandier, J. S. Miller, and R. A. Dressler, J. Chem. Phys. **119**, 10175 (2003).
[18]X.-M. Qian, T. Zhang, Y.-H. Chiu, D. J. Levandier, J. S. Miller, R. A. Dressler, and C. Y. Ng, J. Chem. Phys. **118**, 2455 (2003).
[19]A. N. Panda and N. Sathyamurthy, J. Chem. Phys. **122**, 054304 (2005).
[20]X. N. Tang, H. Xu, T. Zhang, Y. Hou, C. Chang, C. Y. Ng, Y. Chiu, R. A. Dressler, and D. J. Levandier, J. Chem. Phys. **122**, 164301 (2005).
[21]A. N. Panda and S. C. Althorpe, Chem. Phys. Lett. **419**, 245 (2006).
[22]R. A. Dressler, Y. Chiu, D. J. Levandier, X. N. Tang, Y. Hou, C. Chang, C. Houchins, H. Xu, and C.-Y. Ng, J. Chem. Phys. **125**, 132306 (2006).
[23]J. Xiao, C.-L. Yang, X.-F. Tong, M.-S. Wang, and X.-G. Ma, J. Phys. Chem. A **115**, 1486 (2011).
[24]X. Liu, H. Liu, and Q. Zhang, Chem. Phys. Lett. **507**, 24 (2011).
[25]P. Gamallo, F. Huarte-Larrañaga, and M. González, J. Phys. Chem. A **117**, 5393 (2013).
[26]P. Gamallo, R. Martínez, J. D. Sierra, and M. González, Phys. Chem. Chem. Phys. **16**, 6641 (2014).
[27]T. D. Fridgen and J. M. Parnis, J. Chem. Phys. **109**, 2162 (1998).
[28]T. D. Fridgen and J. M. Parnis, J. Chem. Phys. **109**, 2155 (1998).
[29]S. T. Kim and J. S. Lee, J. Chem. Phys. **110**, 4413 (1999).
[30]J. Lundell, M. Pettersson, and M. Räsänen, Phys. Chem. Chem. Phys. **1**, 4151 (1999).
[31]J. Y. Qu, W. Li, R. Guo, and X. S. Zhao, J. Chem. Phys. **117**, 2592 (2002).
[32]A. N. Panda and N. Sathyamurthy, J. Phys. Chem. A **107**, 7125 (2003).
[33]S. Bhattacharya and A. N. Panda, J. Phys. B **42**, 085201 (2009).
[34]J.-J. Liang, C.-L. Yang, L.-Z. Wang, and Q.-G. Zhang, J. Chem. Phys. **136**, 094307 (2012).
[35]D. Koner, A. Vats, M. Vashishta, and A. N. Panda, Comput. Theor. Chem. **1000**, 19 (2012).
[36]D. Koner and A. N. Panda, J. Phys. Chem. A **117**, 13070 (2013).
[37]T.-S. Chu and K.-L. Han, J. Phys. Chem. A **109**, 2050 (2005).
[38]T.-S. Chu and K.-L. Han, Annu. Rep. Prog. Chem. **108**, 10 (2012).
[39]T.-S. Chu and K.-L. Han, Phys. Chem. Chem. Phys. **10**, 2431 (2008).
[40]M. Hankel, Phys. Chem. Chem. Phys. **13**, 7948 (2011).
[41]R. Padmanaban and S. Mahapatra, J. Phys. Chem. A **110**, 6039 (2006).
[42]K.-L. Yeh, D. Xie, D. H. Zhang, S.-Y. Lee, and R. Schinke, J. Phys. Chem. A **107**, 7215 (2003).
[43]E. J. Rackham, F. Huarte-Larrañaga, and D. E. Manolopoulos, Chem. Phys. Lett. **343**, 356 (2001).
[44]E. J. Rackham, T. González-Lezana, and D. E. Manolopoulos, J. Chem. Phys. **119**, 12895 (2003).
[45]T. González-Lezana, Int. Rev. Phys. Chem. **26**, 29 (2007).
[46]E. Carmona-Novillo, T. González-Lezana, O. Roncero, P. Honvault, J.-M. Launay, N. Bulut, F. J. Aoiz, L. Bañares, A. Trottier, and E. Wrede, J. Chem. Phys. **128**, 014304 (2008).
[47]P. Bargueño, T. González-Lezana, P. Larrégaray, L. Bonnet, J.-C. Rayez, M. Hankel, S. C. Smith, and A. J. H. M. Meijer, J. Chem. Phys. **128**, 244308 (2008).
[48]P. Bargueño, P. G. Jambrina, J. M. Alvariño, M. Menéndez, E. Verdasco, M. Hankel, S. C. Smith, F. J. Aoiz, and T. González-Lezana, Phys. Chem. Chem. Phys. **13**, 8502 (2011).
[49]M. Jorfi, T. González-Lezana, A. Zanchet, P. Honvault, and B. Bussery-Honvault, J. Phys. Chem. A **117**, 1872 (2013).
[50]T. González-Lezana, P. Honvault, and Y. Scribano, J. Chem. Phys. **139**, 054301 (2013).
[51]F. Dayou, P. Larrégaray, L. Bonnet, J.-C. Rayez, P. N. Arenas, and T. González-Lezana, J. Chem. Phys. **128**, 174307 (2008).
[52]D. H. Zhang and J. Z. H. Zhang, J. Chem. Phys. **101**, 3671 (1994).
[53]J. Z. H. Zhang, *Theory and Application of Quantum Molecular Dynamics* (World Scientific, 1999).
[54]G. C. Schatz and A. Kuppermann, J. Chem. Phys. **65**, 4642 (1976).
[55]P. McGuire and D. J. Kouri, J. Chem. Phys. **60**, 2488 (1974).
[56]R. T Pack, J. Chem. Phys. **60**, 633 (1974).
[57]S. Y. Lin and H. Guo, J. Chem. Phys. **119**, 11602 (2003).
[58]H. Tal-Ezer and R. Kosloff, J. Chem. Phys. **81**, 3967 (1984).
[59]R. Chen and H. Guo, J. Chem. Phys. **105**, 3569 (1996).
[60]S. K. Gray and G. G. Balint-Kurti, J. Chem. Phys. **108**, 950 (1998).
[61]R. Chen and H. Guo, Comput. Phys. Commun. **119**, 19 (1999).
[62]V. A. Mandelshtam and H. S. Taylor, J. Chem. Phys. **102**, 7390 (1995).
[63]D. T. Colbert and W. H. Miller, J. Chem. Phys. **96**, 1982 (1992).
[64]J. Z. H. Zhang, J. Chem. Phys. **94**, 6047 (1991).
[65]S. Y. Lin, Z. Sun, H. Guo, D. H. Zhang, P. Honvault, D. Xie, and S.-Y. Lee, J. Phys. Chem. A **112**, 602 (2008).
[66]A. Zanchet, O. Roncero, T. González-Lezana, A. Rodríguez-López, A. Aguado, C. Sanz-Sanz, and S. Gómez-Carrasco, J. Phys. Chem. A **113**, 14488 (2009).
[67]A. J. H. M. Meijer, E. M. Goldfield, S. K. Gray, and G. G. Balint-Kurti, Chem. Phys. Lett. **293**, 270 (1998).
[68]S. C. Althorpe, J. Chem. Phys. **114**, 1601 (2001).
[69]M. Lara, A. Aguado, M. Paniagua, and O. Roncero, J. Chem. Phys. **113**, 1781 (2000).
[70]R. T Pack and G. A. Parker, J. Chem. Phys. **87**, 3888 (1987).
[71]D. E. Manolopoulos, J. Chem. Phys. **85**, 6425 (1986).
[72]A. Aguado and M. Paniagua, J. Chem. Phys. **96**, 1265 (1992).
[73]A. Aguado, M. Paniagua, M. Lara, and O. Roncero, J. Chem. Phys. **107**, 10085 (1997).
[74]T. R. Rao, S. Goswami, S. Mahapatra, B. Bussery-Honvault, and P. Honvault, J. Chem. Phys. **138**, 094318 (2013).
[75]T. González-Lezana and P. Honvault, Int. Rev. Phys. Chem. **33**, 371 (2014).
[76]T. González-Lezana, A. Aguado, M. Paniagua, and O. Roncero, J. Chem. Phys. **123**, 194309 (2005).
[77]N. Marković and G. D. Billing, Chem. Phys. Lett. **248**, 420 (1996).
[78]T. González-Lezana, O. Roncero, P. Honvault, J.-M. Launay, N. Bulut, F. J. Aoiz, and L. Bañares, J. Chem. Phys. **125**, 094314 (2006).
[79]F. J. Aoiz, V. Sáez Rábanos, T. González-Lezana, and D. E. Manolopoulos, J. Chem. Phys. **126**, 161101 (2007).
[80]F. J. Aoiz, T. González-Lezana, and V. Sáez Rábanos, J. Chem. Phys. **127**, 174109 (2007).
[81]M. Lara, A. Aguado, O. Roncero, and M. Paniagua, J. Chem. Phys. **109**, 9391 (1998).
[82]A. Rivero-Santamaría, M. L. González-Martínez, T. González-Lezana, J. Rubayo-Soneira, L. Bonnet, and P. Larrégaray, Phys. Chem. Chem. Phys. **13**, 8136 (2011).